# Comparison of the Biomechanics of the Mouse Astrocytic Lamina Cribrosa Between Glaucoma and Optic Nerve Crush Models

Arina Korneva,[1] Elizabeth C. Kimball,[1] Thomas V. Johnson,[1] Sarah E. Quillen,[1] Mary E. Pease,[1] Harry A. Quigley,[1] and Thao D. Nguyen[1,2]

[1]Glaucoma Center of Excellence, Wilmer Eye Institute, Johns Hopkins University School of Medicine, Baltimore, Maryland, United States
[2]Department of Mechanical Engineering, The Johns Hopkins University, Baltimore, Maryland, United States

Correspondence: Arina Korneva, Norris Hall 228, Virginia Tech, 495 Old Turner St., Blacksburg, VA 24061, USA; akorneva@vt.edu.

**Received:** February 20, 2023
**Accepted:** November 14, 2023
**Published:** December 13, 2023

Citation: Korneva A, Kimball EC, Johnson TV, et al. Comparison of the biomechanics of the mouse astrocytic lamina cribrosa between glaucoma and optic nerve crush models. *Invest Ophthalmol Vis Sci.* 2023;64(15):14. https://doi.org/10.1167/iovs.64.15.14

**Purpose.** The strain response of the mouse astrocytic lamina (AL) to an ex vivo mechanical test was compared between two protocols: eyes that underwent sustained intraocular pressure (IOP) increase and eyes after optic nerve crush.

**Methods.** Chronic IOP elevation was induced by microbead injection or the optic nerve was crushed in mice with widespread green fluorescence. After 3 days or 6 weeks, eyes were inflation tested by a published method of two-photon fluorescence to image the AL. Digital volume correlation was used to calculate strains. Optic nerve axon damage was also evaluated.

**Results.** In the central AL but not the peripheral AL, four strains were greater in eyes at the 3-day glaucoma time point than control ($P$ from 0.029 to 0.049, $n = 8$ eyes per group). Also, at this time point, five strains were greater in the central AL compared to the peripheral AL ($P$ from 0.041 to 0.00003). At the 6-week glaucoma time point, the strains averaged across the specimen, in the central AL, and the peripheral AL were indistinguishable from the respective controls. Strains were not significantly different between controls and eyes 3 days or 6 weeks after crush ($n = 8$ and 16).

**Conclusions.** We found alterations in the ex vivo mechanical behavior in eyes from mice with experimental glaucoma but not in those with crushed optic nerves. The results of this study demonstrate that significant axon injury does not directly affect mechanical behavior of the astrocytic lamina.

Keywords: glaucoma, optic nerve, crush, astrocyte, strain, intraocular pressure

Glaucoma is the second leading cause of blindness worldwide.[1] Experimental models of glaucoma in monkey, rat, and mouse show that increased intraocular pressure (IOP) leads to injury to retinal ganglion cell axons at the optic nerve head (ONH) region,[2–6] as is found in human glaucoma eyes.[7] The mouse ONH consists of an astrocytic lamina (AL) whose largely glial structure has similar structural features to the human ONH but without the connective tissue beams of the human ONH.[8] The cellular and connective tissues of the optic nerve head in human eyes with glaucoma remodel in a characteristic manner.[9,10] The more susceptible regions for axon injury correspond to ONH zones with a lower density of supportive tissue,[7,11] and these areas strain more with IOP-generated stress in postmortem human eyes.[12] Reduction in connective beam thickness and decrease in astrocyte area coverage of the human glaucoma lamina cribrosa (LC) are features of more advanced disease.[13] Deformation of the ONH caused by a change in IOP in the living human eye has been estimated using optical coherence tomography (OCT).[14–19] The studies suggest from cross-sectional data that the more advanced the glaucoma, the greater the strains due to a change in the IOP, specifically the greater the maximum principal and maximum shear strains,[17] the greater the effective strain,[18] and the greater the anterior–posterior strain.

The clinical appearance of glaucomatous optic neuropathy is described as excavation or cupping, since the ONH tissues are reduced, are compressed, and move posteriorly and under Bruch's membrane.[20] By contrast, in other optic neuropathies, loss of ganglion cell axons does not lead to a similar clinical appearance, as the visible ONH becomes pale in color but is not excavated.[21] Histologic study of experimental optic nerve transection injury shows dramatically different features from experimental glaucoma in monkey.[22]

Despite the differences between traumatic orbital optic nerve injury and experimental or human glaucomatous optic neuropathy, nerve damage models, particularly crushing the nerve with forceps, are used extensively in ophthalmic research. This derives from the ease of performing crush and from the relatively consistent killing of ganglion cells. Indeed, neuroprotection studies suggest that some beneficial treatments perform similarly in nerve crush and elevated

IOP models.[23] However, other potential neuroprotective therapies for experimental glaucoma have no effect on damage from nerve crush.[24] Astrocytes in the optic nerve are activated in both experimental models with some similarities.[25] The effect of astrocyte activation and remodeling responses on the material properties of the optic nerve head, the site of initial injury in glaucoma, are unknown. While we did not measure material properties, we previously found that strains in the mouse AL increase with 3 days of chronic IOP elevation but decrease 6 weeks later.[26] These dynamic strain alterations are consistent with temporary loss of astrocytic attachment to their basement membrane at the peripapillary sclera.[27]

Retinal ganglion cell degeneration is faster and more severe in the nerve crush model compared to the microbead injection model of glaucoma.[28] In the experimental glaucoma model, astrocytes may be stimulated by the chronic IOP-generated stress or strain in the optic nerve head. Our hypothesis is that the strain response of the AL to ex vivo IOP would be altered in a different way in the crush model compared to the experimental glaucoma model because of the presence of the long-term in vivo IOP elevation in the latter. If the hypothesis were confirmed, it would suggest that IOP elevation or associated stresses stimulate additional tissue responses distinct from the loss of retinal ganglion cell axons alone, which occurs in both models.

To address this, we will use a previously developed method to measure, ex vivo, the strain in the AL due to raising IOP of an explanted eye. We previously showed that the ex vivo strain response in the mouse AL and peripapillary sclera increases following days of in vivo IOP elevation in an experimental model of glaucoma.[26] A similar alteration in the strain response was produced by short-term trypsin treatment to detach the astrocyte processes from the basement membrane.[29] In this study, we measure the strain response of the AL to ex vivo IOP elevation in eyes of experimental mice. We compare the strain response between the experimental glaucoma and the optic nerve crush at both 3 days and 6 weeks after initiation of the models.

## Methods

### Animal Procedures

All experimental procedures were approved and monitored by the Johns Hopkins University School of Medicine Animal Care and Use Committee and adhere to the ARVO Statement for the Use of Animals. Adult mice (4–8 months old), expressing green fluorescent protein in all cells of the body, were used. These were heterozygotes from the cross of C57BL/6 with C57BL/6-Tg (CAG-EGFP)1Osb/J (Pan-GFP, Jackson strain #3291; The Jackson Laboratory, Bar Harbor, ME, USA). For the chronic IOP elevation model, one eye was injected with microbeads following an established protocol.[30] For the optic nerve crush model, the orbital optic nerve was compressed for 5 seconds with cross-action forceps cephalad to the entry of the central retinal artery. Fellow, untreated eyes were used as controls.

IOP was measured as a mean of six readings using the TonoLab rebound tonometer (Tiolat, Inc., Helsinki, Finland) before microbead injection, immediately after injection, and then 1, 2, 3, 7, and 21 days and 6 weeks later. For IOP measurements only, animals were anesthetized using a Rodent Circuit Controller (VetEquip, Inc., Pleasanton, CA, USA) delivering 2.5% of isoflurane in oxygen, 500 cc/min. For eyes followed for 3 days and then sacrificed, we calculated both daily mean IOP and the average of the IOP increase from days 1 to 3. For eyes followed for 6 weeks, we calculated the cumulative difference in IOP between the injected and the fellow eye of each mouse integrated over the 6-week time period (called the positive integral IOP).[31]

Mice were euthanized by an intraperitoneal injection of ketamine/xylazine/acepromazine solution: 50 mg/kg ketamine (Fort Dodge Animal Health, Fort Dodge, IA, USA), 10 mg/kg xylazine (VedCo Inc., Saint Joseph, MO, USA), and 2 mg/kg acepromazine (Phoenix Pharmaceuticals, Burlingame, CA, USA). Mouse eyes were explanted and their optic nerves were removed with a sharp blade posterior to the sclera but anterior to the myelinated nerve portion. The myelinated nerve was placed in paraformaldehyde fixative for epoxy embedding and subsequent quantification of axon loss. The enucleated eyes' anterior–posterior length and width (the width equivalent to the diameter across the ocular equator) were measured with digital calipers (Table 1).

### Inflation Testing

Inflation of explanted eyes was performed according to a published protocol.[32] Briefly, the cornea of the intact eye globe was glued to a plastic holder, and the anterior chamber was cannulated with a needle connected to a fluid reservoir whose height was used to regulate the IOP during inflation testing (Supplementary Fig. S1). The holder and eye were maintained in phosphate-buffered saline at room temperature throughout the experiment. Two images were acquired at IOP = 10 mm Hg and one at IOP = 30 mm Hg, with 15 minutes of equilibration at each pressure. The two images at IOP = 10 mm Hg were compared to estimate baseline error. Images in this study were all taken within the AL. The peripapillary sclera of C57BL/6 mice contains signifi-

**Table 1.** Ocular Axial Length and Width Change

| Group | *N* | Length | Width | % Increase | | Versus Control (*p*) | |
|---|---|---|---|---|---|---|---|
| | | | | Length | Width | Length | Width |
| Control glaucoma | 14 | 3.35 ± 0.09 | 3.37 ± 0.04 | | | | |
| 3-day glaucoma | 6 | 3.49 ± 0.08 | 3.48 ± 0.09 | 4.2 | 3.3 | 0.06 | 0.10 |
| 6-week glaucoma | 8 | 3.81 ± 0.04 | 3.59 ± 0.04 | 13.7 | 6.5 | 0.03* | 0.15 |
| Control crush | 24 | 3.31 ± 0.08 | 3.28 ± 0.07 | | | | |
| 3-day crush | 8 | 3.32 ± 0.80 | 3.25 ± 0.80 | 0.30 | –0.91 | 0.22 | 0.77 |
| 6-week crush | 16 | 3.35 ± 0.12 | 3.32 ± 0.10 | 0.90 | 0.12 | 0.82 | 0.12 |

Values given as mean ± SD (mm); *P* values were from *t*-tests.
* $P \leq 0.05$.

Investigative Ophthalmology & Visual Science

cant melanin pigment, which interferes with the collection of the two-photon fluorescence (TPF) signal in this region.

Images were acquired with a Zeiss laser scanning microscope 710 (Carl Zeiss Microscopy, LLC, Thornwood, NY, USA), with a 20× W Plan Apochromat objective, numerical aperture 1.0. The field of view was excited using a two-photon laser source, excitation wavelength of 895 nm, and collection of TPF signal with a 500- to 550-nm bandpass filter. The z-stacks of 40 to 100 µm spaced every 1 µm were collected with an estimated total $x$- and $y$-resolution of 0.415 µm/pixel. Image postprocessing was performed with a deconvolution algorithm (Huygens Essential; Scientific Volume Imaging, Hilversum, The Netherlands) and contrast enhancement histogram equalization using FIJI.[12,33]

In the overall study, we initiated the experimental protocols with a total of 64 mice, 34 in the glaucoma protocol and 30 in the crush protocols. The final groups with completed data from imaging and analysis were 8 control (contralateral) eyes, 16 glaucoma model eyes, and 24 nerve crush eyes. The remaining eyes/mice did not survive anesthesia, were sacrificed due to presumed pain from cornea defects, or had unsuccessful cannulation and inflation.

### Digital Volume Correlation

The digital volume correlation (DVC) algorithm by Bar-Kochba et al.[34,35] was used to compute the displacement field from the postprocessed images every 1.66 µm in $x$ and $y$ and every 2 µm in $z$. Briefly, the algorithm imports the reference and deformed z-stack volume images. The algorithm divides each volume image into a grid of overlapping three-dimensional (3D) interrogation windows. The algorithm output is a 3D displacement field, where each displacement was calculated by the algorithm matching up the baseline and deformed interrogation windows with a maximum cross-correlation coefficient.[35] The same procedure as in our previous publication[26] was employed to process the 3D displacement field and its 3D displacement gradient tensor. Briefly, data points with an image cross-correlation coefficient by Bar-Kochba et al.[35] $\leq$0.001 were removed. The displacement gradient tensor was used to calculate the 3D Green–Lagrange strain tensor, $\boldsymbol{E}$. The maximum and minimum principal strains, $E_{max}$ and $E_{min}$, in the $x$-$y$ plane were calculated by finding the eigenvalues of the in-plane strain tensor. Maximum shear strain, $\gamma_{max}$, in the $x$-$y$ plane was computed by $\frac{1}{2}(E_{max} - E_{min})$ (Supplementary Table S1). The uncertainty and accuracy of DVC strains were estimated for every specimen by artificially warping one 10-mm Hg image with an applied strain as previously described (Supplementary Table S2).

### Strain Analysis

In the Cartesian coordinate system, the inferior–superior axis of the ONH was identified based on the typical location of inferior blood vessels, and the strain tensor component matrix, $\boldsymbol{E}$, was rotated, such that $x$ = nasal–temporal axis, and $y$ = inferior–superior axis. The components of $\boldsymbol{E}$ greater than the resolution of the DVC (see "Digital Volume Correlation") were $E_{xx}$, $E_{yy}$, $E_{xy}$, and $E_{zz}$. The strain tensor was also transformed to the cylindrical coordinate system with the origin at the geometric center of the AL, such that $r$ indicates radial projections from the geometric center of the AL, and $\theta$ indicates circumferential projections around the AL. In the cylindrical coordinate system, the components of $\boldsymbol{E}$ greater than the baseline DVC error (see "Digital Volume Correlation") were $E_{rr}$, $E_{r\theta}$, $E_{\theta\theta}$ , and $E_{zz}$. The specimen-averaged strain refers to the mean of all points in the AL. In addition, the mean of points in the central region and the mean of points in the peripheral region were computed as follows. To divide the AL into central and peripheral regions, an ellipse was drawn at the external limit of AL, and an inner ellipse was drawn with major and minor axes half of the external ellipse. Sensitivity analysis was used to identify the minimum percentage of DVC-correlated points for a region to be included for statistical analysis.

### Assessment of Axon Loss

After explanation of the eye, the excised optic nerves were immersed in 4% paraformaldehyde in 0.1 M phosphate buffer and $Na_3PO_4$, postfixed in 1% osmium tetroxide ($OsO_4$), and embedded in epoxy resin. The embedded nerve cross sections were cut at a 1-µm thickness from the myelinated portion of the nerve and labeled with 1% toluidine blue. In optic nerve crush eyes, the sections were closer to the globe than the crushed segment. The optic nerves were graded for degree of nerve damage using a semiquantitative method developed for rodent experimental glaucoma and extensively used in mouse glaucoma models.[36,37] An experienced observer (HQ) graded nerves as normal or mild, moderate, or severe damage. In "severe damage" grade nerves, nearly all visible axons were densely stained due to degeneration, and the astrocytes exhibited gliosis. The nerves from both 3-day and 6-week crush eyes were graded, as were the 6-week microbead injected eyes. The 3-day glaucoma eyes were not graded, as damage in this model proceeds more slowly than after crush and would not represent adequately the degree of ultimate damage.[27,38]

### Statistical Methods

Student's $t$-tests were used to compare mean in vivo IOP, ex vivo axial length and width, and ex vivo strain measures in untreated control eyes to microbead injected and to nerve crush eyes. The ten outcome strain measures were $E_{rr}$, $E_{\theta\theta}$, $E_{r\theta}$, $E_{xx}$, $E_{yy}$, $E_{xy}$, $E_{zz}$, $E_{max}$, $E_{min}$, and $\gamma_{max}$ (Supplementary Table S1). Tests to ensure that the distribution of values was normal were performed. In a few examples, one outlier value produced a skewed distribution. In these cases, nonparametric tests were performed, but the significance of the outcome was unaffected. Thus, the $t$-test results are reported here. The relationships between ex vivo strains induced by the inflation test and either the in vivo IOP exposure or the ex vivo axial length or width changes were assessed using linear regression analysis. A significance level of 0.05 was used.

## Results

### Intraocular Pressure Exposure

The mean in vivo IOP of microbead-injected eyes rose significantly above that of fellow, untreated eyes and the differences were statistically significant at 1, 2, 3, and 7 days ($P < 0.001$; Fig. 1). The mean in vivo IOPs of nerve crush eyes were slightly lower than their untreated fellow eyes at 1 and 3 days after crush procedure: 1 day: 16.4 ± 3.5 mm Hg for control (contralateral) versus 11.2 ± 3.1 mm Hg for crush eyes ($P < 0.0001$) and at 3 days: 14.7 ± 4.4 mm Hg for control (contralateral) versus 12.6 ± 2.3 mm Hg for crush

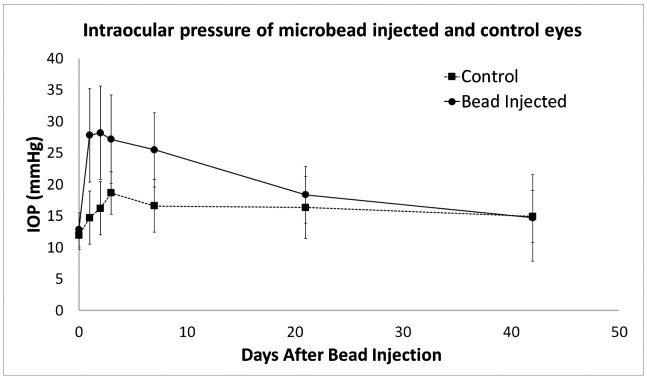


**Figure 1.** Intraocular pressure of microbead-injected and control eyes. The mean IOPs of microbead-injected and control groups show significantly higher IOP in experimental glaucoma eyes at 1 to 7 days ($P \leq 0.05$, *t*-test).

eyes ($P = 0.040$). At other times until sacrifice, the crush and control eyes did not differ significantly from each other or from the baseline in vivo IOP for the group.

The ex vivo length and width of microbead-injected eyes were not statistically different from control eyes after 3 days of elevated in vivo IOP. The eyes after 6 weeks of elevated IOP were significantly longer than control eyes (Table 1, $P \leq 0.03$). There were no significant changes in ex vivo axial length or width in either the 3-day or the 6-week crush group compared to controls.

## Specimen-Averaged Strain

Strains due to the ex vivo IOP increase were averaged across each AL specimen (Fig. 2). Strains exceeded baseline and correlation errors for all strains except the in-plane shear strains, $E_{r\theta}$ and $E_{xy}$ (Supplementary Table S2). The specimen-averaged strains of the 3-day glaucoma eyes were compared to the strains of the control eyes, and none of the comparisons was statistically significant (Tables 2 and 3). Likewise, strains in 6-week glaucoma eyes did not differ from control eyes. $E_{\theta\theta}$ of 6-week glaucoma eyes was significantly lower than $E_{\theta\theta}$ of 3-day glaucoma eyes.

Strains averaged across each AL specimen of the two crush groups, 3 days after crush and 6 weeks after crush, were compared to the same control group, and none significantly exceeded control values (Table 3). Likewise, the strains at 6 weeks after crush were not significantly different from controls. The specimen-averaged strains were also compared between the two crush groups. The strains $E_{rr}$, $E_{max}$, and $\gamma_{max}$ were lower in the 6-week compared to the 3-day crush group eyes.

## Strain Comparison Between the Central and Peripheral AL

Strains were also averaged independently across the central AL and across the peripheral AL for regional comparison of the strain response. In control eyes, there were no significant differences between strains in the central compared to the peripheral AL (Table 4). The 3-day glaucoma group had substantially greater $E_{rr}$, $E_{xx}$, and $E_{yy}$, centrally than peripherally (Table 4), while $\gamma_{max}$ was significantly greater peripherally than centrally. The minimum principal strain in the central AL was positive (tensile) in the 3-day glaucoma group but was negative (compressive) in the peripheral AL of all groups. $E_{rr}$, $E_{\theta\theta}$, $E_{xx}$, and $E_{yy}$ in the central AL of the 3-day glaucoma group were significantly greater than in the central AL of the control group.

In the 6-week glaucoma group, the strains of the AL were not significantly different between the central and peripheral regions. None of the strains in the central AL or in the peripheral AL were significantly different from the respective regional strains of the control group. However, the $E_{rr}$, $E_{\theta\theta}$, $E_{xx}$, and $E_{yy}$ in the central AL of the 6-week glaucoma group were significantly lower than in the central AL of the 3-day glaucoma group (Table 4).

Strains 3 days after nerve crush did not significantly differ between strains of the central compared to the peripheral AL, except in $\gamma_{max}$, which was statistically greater than in the peripheral AL of the control group (Table 5). None of the strains in the central AL or in the peripheral AL in crush eyes was significantly different from the respective regional strains of the control group. The increases in the regional strains of the 3-day glaucoma AL were not present in the 3-day crush group.

In the 6-week crush group, the strains of the AL were not significantly different between the central and peripheral regions. None of the strains was significantly different from the respective central or peripheral strains of the control group (Table 5). The principal strains, $E_{max}$, $E_{min}$, and $\gamma_{max}$, at 6 weeks were significantly lower than those at 3 days after crush.

**Table 2.** Specimen-Averaged Strain in Control and Glaucoma Groups

| Strain | Control, Mean ± SD, % | 3-Day Glaucoma, Mean ± SD, % | 3 Days vs. Control (*P*) | 6-Week Glaucoma, Mean ± SD, % | 6 Weeks vs. Control (*P*) | 3 Days vs. 6 Weeks (*P*) |
|---|---|---|---|---|---|---|
| $E_{rr}$ | 2.61 ± 4.34 | 1.56 ± 2.48 | 0.57 | 2.93 ± 4.78 | 0.89 | 0.48 |
| $E_{\theta\theta}$ | 3.01 ± 2.76 | 6.30 ± 3.51 | 0.06 | 2.80 ± 2.36 | 0.88 | 0.03* |
| $E_{r\theta}$ | 0.16 ± 1.54 | 0.34 ± 1.39 | 0.82 | −1.22 ± 2.27 | 0.17 | 0.12 |
| $E_{xx}$ | 2.91 ± 2.41 | 4.63 ± 2.83 | 0.21 | 2.48 ± 0.78 | 0.64 | 0.06 |
| $E_{yy}$ | 2.70 ± 2.29 | 3.23 ± 3.29 | 0.71 | 3.26 ± 3.36 | 0.71 | 0.99 |
| $E_{xy}$ | −0.05 ± 1.27 | −0.65 ± 0.57 | 0.24 | 0.07 ± 0.84 | 0.83 | 0.06 |
| $E_{zz}$ | 1.42 ± 2.94 | 0.44 ± 0.99 | 0.39 | 1.01 ± 3.05 | 0.79 | 0.62 |
| $E_{max}$ | 9.71 ± 8.60 | 10.45 ± 5.47 | 0.84 | 11.51 ± 10.38 | 0.71 | 0.80 |
| $E_{min}$ | −4.10 ± 4.93 | −2.58 ± 1.76 | 0.43 | −5.77 ± 6.95 | 0.59 | 0.23 |
| $\gamma_{max}$ | 6.90 ± 6.64 | 6.51 ± 3.10 | 0.88 | 8.64 ± 8.62 | 0.66 | 0.52 |

$E_{r\theta}$ and $E_{xy}$ shear strains do not exceed the baseline and correlation errors. Values given as mean ± SD; *P* values were from *t*-tests. $N = 8$ eyes per group.
* $P \leq 0.05$.

Investigative Ophthalmology & Visual Science

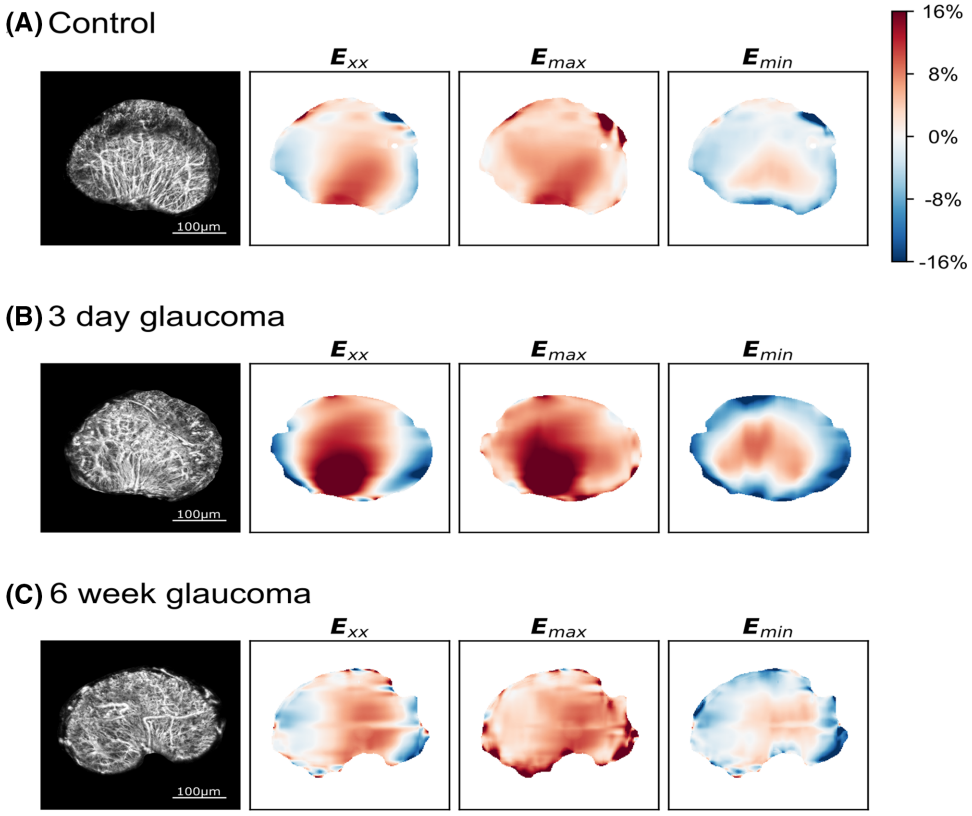


**Figure 2.** Image of the AL and color contours of the strains for representative specimens. *Left to right*: Maximum projection of the image volume of the AL, strains $E_{xx}$, $E_{max}$, $E_{min}$. Plotted strains are means of all z-slices. Strain color bar is the same for all panels and ranges from −16% (*blue*, compressive) to 16% (*red*, tensile) strain. *Image scale bars*: 100 µm.

**Table 3.** Specimen-Averaged Strains in Control and Crush Groups

| Strain | Control, Mean ± SD, % | 3-Day Crush, Mean ± SD, % | 3 Days vs. Control (*P*) | 6-Week Crush, Mean ± SD, % | 6 Weeks vs. Control (*P*) | 3 Days vs, 6 Weeks (*P*) |
|---|---|---|---|---|---|---|
| $E_{rr}$ | 2.61 ± 4.34 | 4.61 ± 4.54 | 0.38 | 1.61 ± 2.38 | 0.47 | 0.044* |
| $E_{\theta\theta}$ | 3.01 ± 2.76 | 6.66 ± 4.65 | 0.08 | 3.72 ± 4.03 | 0.66 | 0.12 |
| $E_{r\theta}$ | 0.16 ± 1.54 | −0.18 ± 1.51 | 0.65 | 0.52 ± 1.91 | 0.66 | 0.38 |
| $E_{xx}$ | 2.91 ± 2.41 | 6.48 ± 5.50 | 0.11 | 3.07 ± 3.18 | 0.90 | 0.065 |
| $E_{yy}$ | 2.70 ± 2.29 | 4.78 ± 3.62 | 0.19 | 2.26 ± 3.78 | 0.77 | 0.13 |
| $E_{xy}$ | −0.05 ± 1.27 | 0.72 ± 0.92 | 0.19 | 0.35 ± 1.64 | 0.56 | 0.56 |
| $E_{zz}$ | 1.42 ± 2.94 | 1.54 ± 1.92 | 0.92 | 0.53 ± 1.26 | 0.31 | 0.14 |
| $E_{max}$ | 9.71 ± 8.60 | 18.25 ± 12.35 | 0.13 | 8.82 ± 8.41 | 0.81 | 0.037* |
| $E_{min}$ | −4.10 ± 4.93 | −6.99 ± 5.27 | 0.28 | −3.49 ± 3.72 | 0.74 | 0.072 |
| $\gamma_{max}$ | 6.90 ± 6.64 | 12.62 ± 8.41 | 0.15 | 6.15 ± 5.79 | 0.78 | 0.037* |

$E_{r\theta}$ and $E_{xy}$ shear strains do not exceed the baseline and correlation errors. Values given as mean ± SD; *P* values from *t*-tests. $N = 8$ eyes in control group, 8 eyes in the 3-day group, and 16 eyes in the 6-week group.
* $P \leq 0.05$.

## Relationship Between Strains, IOP Exposure, and Axial Length Change in Glaucoma Eyes

For the eyes in the 3-day and 6-week glaucoma groups, we analyzed the relationship between either the in vivo IOP exposure or the ex vivo axial length change to strains induced by the inflation test. Specimen-averaged strains, strains averaged in the central AL, and strains averaged in the peripheral AL were assessed. The difference in the specimen-averaged $E_{\theta\theta}$ between 3 days and 6 weeks was statistically significant (Table 2). However, the 3-day IOP average was not significantly related to the specimen-averaged $E_{\theta\theta}$ for each eye by linear regression (data not shown). For microbead-injected eyes followed for 6 weeks, we compared the cumulative IOP exposure, positive integral IOP, to the specimen-averaged $E_{\theta\theta}$, but the linear regression analysis showed no significant association ($P > 0.5$). The relationship between the specimen-averaged $E_{\theta\theta}$ increasing with greater axial length in the 6-week glaucoma group was not statistically significant by linear regression ($R^2 = 0.18$, $P = 0.30$, linear regression; Fig. 3).

Investigative Ophthalmology & Visual Science

**Table 4.** Strain Comparison Between the Central and Peripheral AL in Control and Glaucoma Groups

| | | | | | | 3-Day Glaucoma vs. Control | | | | 6-Week Glaucoma vs. Control | | 3-Day Glaucoma vs. 6-Week Glaucoma | |
|---|---|---|---|---|---|---|---|---|---|---|---|---|---|
| **Strain** | **Region** | **Control, Mean ± SD, %** | **C vs. P (*P*)** | **3-Day Glaucoma, Mean ± SD, %** | **C vs. P (*P*)** | **Central (*P*)** | **Peripheral (*P*)** | **6-Week Glaucoma, Mean ± SD, %** | **C vs. P (*P*)** | **Central (*P*)** | **Peripheral (*P*)** | **Central (*P*)** | **Peripheral (*P*)** |
| $E_{rr}$ | Central | 2.45 ± 2.96 | | 6.56 ± 3.76 | | 0.029* | | 1.60 ± 4.34 | | 0.65 | | 0.028* | |
| | Peripheral | 1.85 ± 5.22 | 0.82 | −1.78 ± 1.57 | <0.001* | | 0.08 | 3.91 ± 11.47 | 0.60 | | 0.65 | | 0.19 |
| $E_{\theta\theta}$ | Central | 2.70 ± 5.16 | | 7.98 ± 4.43 | | 0.045* | | 2.36 ± 5.36 | | 0.90 | | 0.039* | |
| | Peripheral | 2.94 ± 2.90 | 0.81 | 5.27 ± 3.05 | 0.17 | | 0.14 | 3.18 ± 1.71 | 0.68 | | 0.84 | | 0.11 |
| $E_{xx}$ | Central | 2.86 ± 6.57 | | 9.00 ± 4.69 | | 0.049* | | 2.15 ± 7.60 | | 0.85 | | 0.048* | |
| | Peripheral | 2.60 ± 3.81 | 0.84 | 2.18 ± 1.57 | 0.002* | | 0.78 | 2.78 ± 5.56 | 0.85 | | 0.94 | | 0.77 |
| $E_{yy}$ | Central | 2.29 ± 2.09 | | 5.54 ± 3.72 | | 0.049* | | 1.81 ± 2.27 | | 0.66 | | 0.029* | |
| | Peripheral | 2.18 ± 2.12 | 0.96 | 1.31 ± 2.10 | 0.014* | | 0.42 | 4.31 ± 6.85 | 0.34 | | 0.41 | | 0.25 |
| $E_{zz}$ | Central | 0.54 ± 2.26 | | −0.08 ± 1.34 | | 0.518 | | 0.26 ± 3.05 | | 0.84 | | 0.77 | |
| | Peripheral | 1.87 ± 3.04 | 0.94 | 0.54 ± 1.06 | 0.33 | | 0.26 | 1.81 ± 3.36 | 0.35 | | 0.97 | | 0.33 |
| $E_{max}$ | Central | 6.88 ± 3.86 | | 11.73 ± 5.20 | | 0.053 | | 8.39 ± 4.82 | | 0.50 | | 0.20 | |
| | Peripheral | 10.55 ± 9.44 | 0.84 | 9.07 ± 4.69 | 0.29 | | 0.70 | 13.91 ± 16.24 | 0.37 | | 0.62 | | 0.43 |
| $E_{min}$ | Central | −1.73 ± 7.01 | | 2.82 ± 3.17 | | 0.117 | | −4.43 ± 10.06 | | 0.54 | | 0.07 | |
| | Peripheral | −5.77 ± 4.78 | 0.91 | −5.58 ± 2.21 | <0.001* | | 0.92 | −6.82 ± 5.97 | 0.57 | | 0.71 | | 0.59 |
| $\gamma_{max}$ | Central | 4.31 ± 3.99 | | 4.46 ± 1.37 | | 0.922 | | 6.41 ± 6.25 | | 0.44 | | 0.40 | |
| | Peripheral | 8.16 ± 7.05 | 0.09 | 7.32 ± 3.31 | 0.041* | | 0.77 | 10.36 ± 10.64 | 0.38 | | 0.63 | | 0.45 |

Values given as mean ± SD; *P* values from *t*-tests. $N = 8$ eyes per group. C, central; P, peripheral.
* $P \leq 0.05$.

**Table 5.** Strain Comparison Between the Central and Peripheral AL in Control and Crush Groups

| | | | | | | 3-Day Crush vs. Control | | | | 6-Week Crush vs. Control | | 3-Day Crush vs. 6-Week Crush | |
|---|---|---|---|---|---|---|---|---|---|---|---|---|---|
| **Strain** | **Region** | **Control, Mean ± SD, %** | **C vs. P (*P*)** | **3-Day Crush, Mean ± SD, %** | **C vs. P (*P*)** | **Central (*P*)** | **Peripheral (*P*)** | **6-Week Crush, Mean ± SD, %** | **Strain** | **Region** | **Control, Mean ± SD, %** | **C vs. P (*P*)** | **3-Day Crush, Mean ± SD, %** |
| $E_{rr}$ | Central | 2.45 ± 2.96 | | 4.50 ± 4.49 | | 0.30 | | 3.10 ± 4.08 | | 0.69 | | 0.45 | |
| | Peripheral | 1.85 ± 5.22 | 0.82 | 4.69 ± 5.20 | 0.90 | | 0.29 | 1.69 ± 4.10 | 0.38 | | 0.94 | | 0.14 |
| $E_{\theta\theta}$ | Central | 2.70 ± 5.16 | | 5.30 ± 3.88 | | 0.27 | | 4.54 ± 5.22 | | 0.42 | | 0.72 | |
| | Peripheral | 2.94 ± 2.90 | 0.81 | 7.29 ± 5.65 | 0.77 | | 0.07 | 3.86 ± 4.27 | 0.09 | | 0.59 | | 0.11 |
| $E_{xx}$ | Central | 2.86 ± 6.57 | | 6.91 ± 5.45 | | 0.20 | | 3.63 ± 4.50 | | 0.74 | | 0.13 | |
| | Peripheral | 2.60 ± 3.81 | 0.84 | 6.19 ± 5.87 | 0.25 | | 0.17 | 3.46 ± 3.99 | 0.42 | | 0.62 | | 0.19 |
| $E_{yy}$ | Central | 2.29 ± 2.09 | | 2.89 ± 3.34 | | 0.67 | | 4.01 ± 5.21 | | 0.38 | | 0.59 | |
| | Peripheral | 2.18 ± 2.12 | 0.96 | 5.79 ± 5.13 | 0.71 | | 0.09 | 2.10 ± 4.88 | 0.85 | | 0.96 | | 0.10 |
| $E_{zz}$ | Central | 0.54 ± 2.26 | | 1.57 ± 2.10 | | 0.36 | | 0.18 ± 2.26 | | 0.72 | | 0.16 | |
| | Peripheral | 1.87 ± 3.04 | 0.94 | 1.44 ± 1.88 | 0.56 | | 0.74 | 0.56 ± 1.45 | 0.88 | | 0.16 | | 0.22 |
| $E_{max}$ | Central | 6.88 ± 3.86 | | 12.28 ± 8.49 | | 0.12 | | 8.80 ± 8.07 | | 0.53 | | 0.34 | |
| | Peripheral | 10.55 ± 9.44 | 0.84 | 21.26 ± 14.63 | 0.11 | | 0.10 | 9.64 ± 10.45 | 0.46 | | 0.84 | | 0.035* |
| $E_{min}$ | Central | −1.73 ± 7.01 | | −2.48 ± 4.53 | | 0.81 | | −1.16 ± 3.77 | | 0.79 | | 0.46 | |
| | Peripheral | −5.77 ± 4.78 | 0.91 | −9.28 ± 5.88 | 0.21 | | 0.21 | −4.09 ± 4.00 | 0.23 | | 0.37 | | 0.018* |
| $\gamma_{max}$ | Central | 4.31 ± 3.99 | | 7.38 ± 5.63 | | 0.23 | | 4.98 ± 4.53 | | 0.73 | | 0.27 | |
| | Peripheral | 8.16 ± 7.05 | 0.09 | 15.27 ± 9.85 | 0.05* | | 0.12 | 6.87 ± 6.94 | 0.13 | | 0.67 | | 0.024* |

Values given as mean ± SD; *P* values from *t*-tests. $N = 8$ eyes per group.
* $P \leq 0.05$.

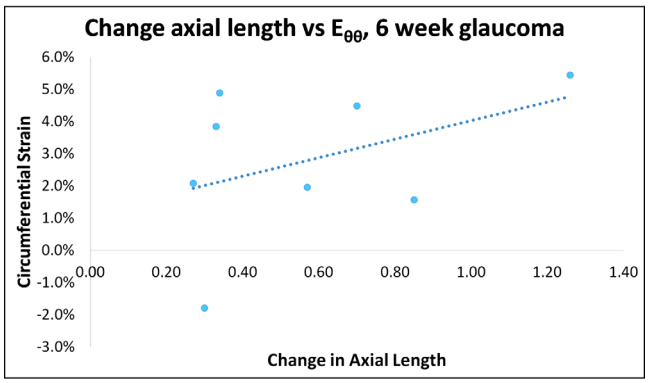


**Figure 3.** Relationship between specimen-averaged $E_{\theta\theta}$ and the change of axial length (mm) for 6-week glaucoma eyes. The increase in axial length by 6 weeks after microbead injection was mildly but not significantly related to the $E_{\theta\theta}$ strain, the strain that was most substantially altered in IOP elevation eyes at 3 days.

We also compared the strains in central and peripheral regions to the mean in vivo IOP increase from 1 to 3 days after microbead injection and to the change in axial length and width of eyes at 3 days after microbead injection. There were no statistically significant relationships (all $P > 0.40$, linear regression). We also compared the strains at 6 weeks after microbead injection in central and peripheral regions to the positive integral of the in vivo IOP and to the increase in axial length and width at 6 weeks. Again, there were no significant relationships detected (all linear regression relationships had $P \geq 0.50$).

### Comparison of Strains to Optic Nerve Axon Damage

The degree of axon loss in masked analysis among nerves after crush was variable at 3 days after injury but substantially greater by 6 weeks (Table 6). Based on previously published data, no substantial axon loss occurs 3 days after microbead injection. By 6 weeks after IOP elevation by microbead injection, most eyes had moderate or severe nerve damage. Among 36 control eyes, most were graded as normal or with mild nerve damage. To determine the effect of axon loss on strain, the specimens were categorized into three groups based on their axon damage grade: normal, mild grouped with moderate, and severe. Specimen-averaged, central, and peripheral strains were not statistically different between the three categories of axon damage in specimens from the 3-day crush group ($n = 12$ normal, $n = 13$ mild plus moderate, and $n = 17$ severe, all $P > 0.27$, pairwise $t$-tests). The strains did not significantly differ between the categories of axon damage in the 6-week crush group ($n = 0$ normal, $n = 6$ mild plus moderate, $n = 10$ severe). Finally, for the 6-week glaucoma group, no significant differences in strains were found after categorizing specimens by nerve damage grade ($n = 1$ normal, $n = 4$ mild plus moderate, $n = 3$ severe).

**Table 6.** Grades for Optic Nerve Axon Loss

| Group | N | Normal | Mild | Moderate | Severe |
|---|---|---|---|---|---|
| Control | 36 | 30 | 5 | 1 | 0 |
| 3-day crush | 8 | 2 | 1 | 2 | 3 |
| 6-week crush | 14 | 0 | 0 | 4 | 10 |
| 6-week glaucoma | 8 | 1 | 2 | 2 | 3 |

## Discussion

The regional strains due to ex vivo IOP elevation in untreated mouse AL were similar in central and peripheral zones, although one of the strains, the maximum principal strain, was somewhat larger peripherally than centrally. One recent study of three monkeys found that premortem strains due to an increase in IOP were somewhat greater than postmortem strains using OCT imaging, specifically the median effective and the maximum shear strains.[39] There are displacements measurable by OCT in human eyes due to vascular pulsation,[40] and these may influence regions of the human ONH or the mouse AL nearer to large vessels. In the human eye, the regional maximum principal strain due to ex vivo inflation test of the posterior scleral cups was greater in upper and lower polar areas of the ONH.[12] This regional strain finding is consistent with the regions where axonal loss is selectively greater,[9] but unlike in the human eye, the regional axon loss is not a strong feature of experimental mouse glaucoma.[41] Thus, it is not surprising that in this study, nasal–temporal, superior–inferior, circumferential, radial, in-plane shear, maximum principal, minimum principal, and maximum shear strains do not differ between the central and peripheral AL in control specimens.

After exposure to increased IOP for 3 days, central AL strains were significantly greater than control, but peripheral strains were not, leading to no statistically significant change in specimen-averaged strains. Interestingly, the peripheral strains were often numerically lower than in controls. Of note, mean $E_{rr}$ actually became compressive (negative; $P = 0.08$ compared to control), while central $E_{rr}$ was significantly more tensile (positive) than control AL. Detailed study of another mouse type with our methods also showed an increase in strains 3 days after IOP increase.[26] The interaction between the mechanics of the peripapillary sclera and AL at this early time point needs to be further investigated to determine the underlying mechanism since scleral stiffness and thickness significantly influence AL mechanics.[42–44] The degree to which scleral biomechanics is altered in the mouse after only 3 days of elevated IOP is unknown. But even in healthy human specimens, a smaller $E_{max}$ of the peripapillary sclera was correlated with a greater posterior displacement of the human LC.[45] In the mouse, after 3 to 7 days of IOP increase, we found separation of peripheral astrocyte processes from their peripheral attachments to the choroid–scleral opening from the AL.[27] A similar structural retraction of astrocytes from peripheral attachments was reported in rat glaucoma.[46] Mechanically, this could be modeled as a reduction in the constraints at the circular edge of a thin circular plate, which would result in greater tensile strain under bending. A smaller circumferential prestrain applied to the edge of the plate, such as from a stiffer sclera, would have a similar effect.

The 6-week glaucoma eyes had strains similar to control values, as did strains at 6 weeks in our prior mouse type.[26] We hypothesize that this may be due to transient changes in astrocyte structure soon after IOP elevation that revert toward normal by 6 weeks,[27] which were also observed after short-term IOP elevation in rat[47,48] models. In addition, in experimental IOP elevation in monkey eyes, a more compliant ONH structural change was observed by OCT at 1 to 2 weeks after IOP elevation that reverted to a less compliant

Investigative Ophthalmology & Visual Science

response months later.[49,50] Our electron microscopic findings in the mouse glaucoma model show that 6 weeks after higher IOP exposure, the astrocytes of the AL have reestablished connections to their peripheral basement membrane at the sclera, along with filling in of pores formerly occupied by axons that have died.[27] These remodeling events seem consistent with a return toward normal AL strain behavior. Others found a stiffer strain response to IOP in the sclera in experimental glaucoma after 6 weeks in mice[51] and before ONH surface changes in monkeys,[52] which according to modeling studies[42–44] may also cause an increase in the AL strain.

The estimated strains in untreated mouse eyes in this experiment were of similar magnitude to those previously measured by our lab using two other mouse types, one of whose astrocytes express green fluorescent protein under control of either the glutamate transporter (GLT1) promoter[53] and one in which the fluorescent marker is driven by the glial fibrillary acidic protein promoter.[29] Some differences among mouse types would be expected, as differences in eye size, pigmentation, genetic factors, and tissue behaviors may affect biomechanical responses.[42,44] The strains reported in human ONH both postmortem[45,54] and in living eyes[15,55] are also generally of similar magnitude, despite the anatomic differences and variations in level and duration of IOP changes.

We have found that various genetic backgrounds of mice differ in susceptibility to experimental glaucoma injury,[56,57] and age-related susceptibility differs among mouse types.[38] Even within the C57BL/6 mouse, the amount of ganglion cell damage from the microbead model has shown considerable variation over several years in our experience. While the variation in the magnitude of strain (strain due to the same ex vivo IOP increase) between mouse genotypes is small in our studies, it is unknown whether these differences in strains would be amplified or diminished in vivo. Differences in the in vivo stresses and strains associated with an increase in IOP may contribute to the severity of the glaucomatous tissue responses across individual mice and across genotypes.

The specimen-averaged central and peripheral strains at both time points after crush injury were not different from control values. This was true despite substantial loss of axons by the 6-week time point. The higher than control values of strain in the central AL were only measured in glaucoma eyes at 3 days and not in the crush eyes. This suggests that the remodeling of the biomechanical behavior of the AL in the glaucoma model is not directly due to axonal injury and later axon loss. Substantial remodeling of the noncollagenous components of the sclera may also contribute to the altered AL strain response at 3 days. The chronic in vivo IOP elevation may stimulate remodeling of the biomechanical behavior of the sclera and the AL in glaucoma models. The viscoelastic material properties of the tissues of the ONH[58–60] may have influenced the IOP-induced stresses experienced by the AL.

Future work is needed to determine the mechanism of remodeling that leads to the increase in the strain response in the IOP-elevated glaucoma model in contrast to the little changes in the crush model. The results of our study do not contradict general findings from primate studies of glaucoma and other optic neuropathies. In experimental monkey models and in human histologic studies, there are clear differences between the effects of chronically elevated IOP and optic neuropathy produced by non-IOP mediated conditions, such as nerve crush/transection or ischemic optic neuropathy.[22,61–63] The clinical appearance of the optic disc with nonglaucomatous atrophy differs from glaucoma,[22,63] and this derives from a failure of the connective beams of the ONH to remodel[22] in nonglaucoma neuropathy. Instead, astrocytes fill in the spaces formerly occupied by axons, leaving the general connective tissue structure intact. In human glaucoma eyes, by contrast, morphologic analysis of the LC beam and pore structure showed that greater glaucoma damage was associated with smaller pores, thinner connective tissue beams, and a greater number of cell nuclei in the LC pores, suggesting a migration of astrocytes into the former axonal bundle pores.[13] In contrast, morphologic analysis of the LC of early glaucoma monkey eyes reported both thinning and thickening of the connective tissue beams, where areas with thinner beams had greater pore diameters, and areas with thicker beams had smaller pore diameters.[64] We are presently comparing the differential gene expression between healthy, crush injury, and glaucoma mouse models[65] to help explain the differences in the ex vivo biomechanical strain behavior found in this study and the differences in the microanatomy found elsewhere.

The present data have some known limitations. We could not include strain data from the sclera, as the mice used are pigmented and the melanin in the peripapillary area precludes second harmonic generation imaging to assess scleral strain. While peripapillary scleral strains in mouse as previously measured are smaller than those of the AL, we have measured significant change in scleral fiber structure in the microbead mouse glaucoma model.[53,66–68] Computational modeling suggests that scleral mechanical behavior interacting with the LC is an important feature in ONH strain.[42–44] Time-dependent material behavior was not examined in the sclera or the astrocytic lamina in our study. The viscoelastic behavior of monkey sclera[60] and the porcine LC[59] exhibits stress–relaxation on the time scale of 200 seconds. Thus, measurement of the time-dependent behavior on the 3-day time scale of the sclera and astrocytic lamina is needed to rule out a possible passive mechanism. Another limitation is that some AL strains ($E_{r\theta}$, $E_{xy}$, and $E_{zz}$) were largely within the DVC-estimated strain error and thus cannot be assessed effectively with these methods. Furthermore, the mouse AL differs from the larger mammalian ONH that has connective tissue beams covered by astrocytes.

While the use of explanted eyes retains the normal architecture within which astrocytes reside, it excludes some relevant loads, such as the effect of optic nerve tissue pressure, optic nerve connective tissue support, and the effect of active blood flow. Therefore, the strain magnitudes calculated herein may not be equivalent to the strain magnitudes in vivo. Characterization of the mechanical behavior of ocular tissues such as the sclera, the choroid, and LC using experimental and computational methods is needed to improve the prediction of in vivo stresses and strains in the optic nerve head. To remedy this, methods were developed by us and others to measure the biomechanical behavior of the ONH in human patients. The strain of the human ONH due to a change in the IOP can now be measured in vivo by using OCT imaging and by various manipulation of the IOP.[14–19,69]

## Conclusions

The strains of the AL to an ex vivo inflation test were greater than control in the central AL after 3 days of in vivo elevated

Investigative Ophthalmology & Visual Science

IOP. The strains after 6 weeks of experimental glaucoma were similar to control. Strain in the AL of eyes 3 days and 6 weeks after optic nerve crush injury did not significantly differ from control values. The ex vivo strain response of the AL was transiently altered in the glaucoma model but was not significantly affected by the optic nerve crush injury. This suggests that chronic IOP elevation of the glaucoma model produces biomechanical effects additional to the RGC axon loss present in both models.

## *Acknowledgments*

Supported by National Institutes of Health grants EY 02120 (HQ), EY 01765 (Core Grant to Wilmer Institute), T32EY007143 (AK), and NSF Award 1727104 (TDN) and unrestricted support from Research to Prevent Blindness, Inc. and from donors to the Glaucoma Center of Excellence.

DVC analysis was performed using the Maryland Advanced Research Computing Center (MARCC).

Disclosure: **A. Korneva**, None; **E.C. Kimball**, None; **T.V. Johnson**, None; **S.E. Quillen**, None; **M.E. Pease**, None; **H.A. Quigley**, None; **T.D. Nguyen**, None

## *References*

1. Tham YC, Li X, Wong TY, Quigley HA, Aung T, Cheng CY. Global prevalence of glaucoma and projections of glaucoma burden through 2040: a systematic review and meta-analysis. *Ophthalmology*. 2014;121(11):2081–2090.
2. Quigley HA, Addicks EM. Chronic experimental glaucoma in primates II. Effect of extended intraocular pressure elevation on optic nerve head and axonal transport. *Invest Ophthalmol Vis Sci*. 1980;19(2):137–152.
3. Pease ME, McKinnon SJ, Quigley HA, Kerrigan-Baumrind LA, Zack DJ. Obstructed axonal transport of BDNF and its receptor TrkB in experimental glaucoma. *Invest Ophthalmol Vis Sci*. 2000;41(3):764–774.
4. Cone FE, Gelman SE, Son JL, Pease ME, Quigley HA. Differential susceptibility to experimental glaucoma among 3 mouse strains using bead and viscoelastic injection. *Exp Eye Res*. 2010;91(3):415–424.
5. Tehrani S, Davis L, Cepurna WO, et al. Optic nerve head astrocytes display axon-dependent and-independent reactivity in response to acutely elevated intraocular pressure. *Invest Ophthalmol Vis Sci*. 2019;60(1):312–321.
6. Morrison JC, Moore CG, Deppmeier LMH, Gold BG, Meshul CK, Johnson EC. A rat model of chronic pressure-induced optic nerve damage. *Exp Eye Res*. 1997;64(1):85–96.
7. Quigley HA, Addicks EM, Green WR, Maumenee AE. Optic nerve damage in human glaucoma: II. The site of injury and susceptibility to damage. *Arch Ophthalmol*. 1981;99(4):635–649.
8. Sun D, Lye-Barthel M, Masland RH, Jakobs TC. The morphology and spatial arrangement of astrocytes in the optic nerve head of the mouse. *J Comp Neurol*. 2009;516(1):1–19.
9. Quigley HA, Green WR. The histology of human glaucoma cupping and optic nerve damage: clinicopathologic correlation in 21 eyes. *Ophthalmology*. 1979;86(10):1803–1827.
10. Varela HJ, Hernandez MR. Astrocyte responses in human optic nerve head with primary open-angle glaucoma. *J Glaucoma*. 1997;6(5):303–313.
11. Quigley HA, Addicks EM. Regional differences in the structure of the lamina cribrosa and their relation to glaucomatous optic nerve damage. *Arch Ophthalmol*. 1981;99(1):137–143.
12. Midgett DE, Pease ME, Jefferys JL, et al. The pressure-induced deformation response of the human lamina cribrosa: analysis of regional variations. *Acta Biomater*. 2017;53:123–139.
13. Guan C, Pease ME, Quillen S, et al. Quantitative microstructural analysis of cellular and tissue remodeling in human glaucoma optic nerve head. *Invest Ophthalmol Vis Sci*. 2022;63(11):18.
14. Girard MJA, Beotra MR, Chin KS, et al. In vivo 3-dimensional strain mapping of the optic nerve head following intraocular pressure lowering by trabeculectomy. *Ophthalmology*. 2016;123(6):1190–1200.
15. Midgett DE, Quigley HA, Nguyen TD. In vivo characterization of the deformation of the human optic nerve head using optical coherence tomography and digital volume correlation. *Acta Biomater*. 2019;96:385–399.
16. Fazio MA, Clark ME, Bruno L, Girkin CA. In vivo optic nerve head mechanical response to intraocular and cerebrospinal fluid pressure: imaging protocol and quantification method. *Sci Rep*. 2018;8(1):12639.
17. Czerpak CA, Kashaf MS, Zimmerman BK, Quigley HA, Nguyen TD. The strain response to intraocular pressure decrease in the lamina cribrosa of glaucoma patients. *Ophthalmol Glaucoma*. 2023;6(1):11–22.
18. Chuangsuwanich T, Tun TA, Braeu FA, et al. Differing associations between optic nerve head strains and visual field loss in patients with normal- and high-tension glaucoma. *Ophthalmology*. 2023;130(1):99–110.
19. Czerpak CA, Ling YTT, Jefferys JL, et al. The curvature, collagen network structure, and their relationship to the pressure-induced strain response of the human lamina cribrosa in normal and glaucoma eyes. *J Biomech Eng*. 2023;145(10):101005-1-1010005-14.
20. Quigley HA, Hohman RM, Addicks EM, Massof RS, Green WR. Morphologic changes in the lamina cribrosa correlated with neural loss in open-angle glaucoma. *Am J Ophthalmol*. 1983;95(5):673–691.
21. Danesh-Meyer HV, Boland MV, Savino PJ, et al. Optic disc morphology in open angle glaucoma compared with anterior ischemic optic neuropathies. *Invest Ophthalmol Vis Sci*. 2010;51(4):2003–2010.
22. Morrison JC, Dorman-Pease ME, Dunkelberger GR, Quigley HA. Optic nerve head extracellular matrix in primary optic atrophy and experimental glaucoma. *Arch Ophthalmol*. 1990;108(7):1020–1024.
23. Welsbie DS, Yang Z, Ge Y, et al. Functional genomic screening identifies dual leucine zipper kinase as a key mediator of retinal ganglion cell death. *Proc Natl Acad Sci USA*. 2013;110(10):4045–4050.
24. Quigley HA, Pitha IF, Welsbie DS, et al. Losartan treatment protects retinal ganglion cells and alters scleral remodeling in experimental glaucoma. *PLoS One*. 2015;10(10):e0141137.
25. Sun D, Moore S, Jakobs TC. Optic nerve astrocyte reactivity protects function in experimental glaucoma and other nerve injuries. *J Exp Med*. 2017;214(5):1411–1430.
26. Korneva A, Kimball EC, Jefferys JL, Quigley HA, Nguyen TD. Biomechanics of the optic nerve head and peripapillary sclera in a mouse model of glaucoma. *J R Soc Interface*. 2020;17(173):20200708.
27. Quillen S, Schaub J, Quigley H, et al. Astrocyte responses to experimental glaucoma in mouse optic nerve head. *PLoS One*. 2020;15(8):e0238104.
28. Kalesnykas G, Oglesby EN, Zack DJ, et al . Retinal ganglion cell morphology after optic nerve crush and experimental glaucoma. *Invest Ophthalmol Vis Sci*. 2012;53(7):3847–3857.
29. Korneva A, Kimball EC, Quillen S, et al. Mechanical strain in the mouse astrocytic lamina increases after exposure to recombinant trypsin. *Acta Biomater*. 2022;163:312–325.

30. Cone FE, Steinhart MR, Oglesby EN, Kalesnykas G, Pease ME, Quigley HA. The effects of anesthesia, mouse strain and age on intraocular pressure and an improved murine model of experimental glaucoma. *Exp Eye Res*. 2012;99(1):27–35.
31. Levkovitch-Verbin H, Quigley HA, Martin KR, Valenta D, Baumrind LA, Pease ME. Translimbal laser photocoagulation to the trabecular meshwork as a model of glaucoma in rats. *Invest Ophthalmol Vis Sci*. 2002;43(2):402–410.
32. Nguyen C, Midgett D, Kimball EC, et al. Measuring deformation in the mouse optic nerve head and peripapillary sclera. *Invest Ophthalmol Vis Sci*. 2017;58(2):721–733.
33. Schindelin J, Arganda-Carreras JI, Frise E, et al. Fiji: an open-source platform for biological-image analysis. *Nat Methods*. 2012;9:676–682.
34. Bar-Kochba E, Toyjanova J, Andrews E, et al. A fast iterative digital volume correlation algorithm for large deformations. *Exp Mech*. 2015;55(1):261–274.
35. Bar-Kochba E, Toyjanova J, Andrews E, et al. A fast iterative digital volume correlation algorithm for large deformations. *GitHub Repository*, https://github.com/FranckLab/FIDVC. Accessed September 1, 2020.
36. Tolman NG, Balasubramanian R, Macalinao DG, et al. Genetic background modifies vulnerability to glaucoma-related phenotypes in Lmx1b mutant mice. *Dis Model Mech*. 2021;14(2):dmm046953.
37. Madhoun S, Martins MTC, Korneva A, et al. Effects of experimental glaucoma in Lama1nmf223 mutant mice. *Exp Eye Res*. 2023;226:109341.
38. Kimball EC, Jefferys JL, Pease ME, et al. The effects of age on mitochondria, axonal transport, and axonal degeneration after chronic IOP elevation using a murine ocular explant model. *Exp Eye Res*. 2018;172(7):78–85.
39. Wei J, Hua Y, Yang B, et al. Comparing acute IOP-induced lamina cribrosa deformations premortem and postmortem. *Transl Vis Sci Technol*. 2022;11(12):1.
40. Solano MM, Richer E, Cheriet F, Lesk MR, Costantino S. Mapping pulsatile optic nerve head deformation using OCT. *Ophthalmology Sci*. 2022;2(4):100205.
41. Schaub JA, Kimball EC, Steinhart MR, et al. Regional retinal ganglion cell axon loss in a murine glaucoma model. *Invest Ophthalmol Vis Sci*. 2017;58(5):2765–2773.
42. Sigal IA, Flanagan JG, Ethier CR. Factors influencing optic nerve head biomechanics. *Invest Opthalmol Vis Sci*. 2005;46(11):4189–4199.
43. Bellezza AJ, Hart RT, Burgoyne CF. The optic nerve head as a biomechanical structure: initial finite element modeling. *Invest Ophthalmol Vis Sci* 2000;41(10):2991–3000.
44. Sigal IA, Yang H, Roberts MD, et al. IOP-induced lamina cribrosa deformation and scleral canal expansion: independent or related? *Invest Ophthalmol Vis Sci* 2011;52(12):9023–9032.
45. Midgett DE, Jefferys JL, Quigley HA, Nguyen TD. The inflation response of the human lamina cribrosa and sclera: analysis of deformation and interaction. *Acta Biomater*. 2020;106(4):225–241.
46. Dai C, Khaw PT, Yin ZQ, et al. Structural basis of glaucoma: the fortified astrocytes of the optic nerve head are the target of raised intraocular pressure. *Glia*. 2012;60(1):13–28.
47. Johnson EC, Deppmeier LMH, Wentzien SKF, et al. Chronology of optic nerve head and retinal responses to elevated intraocular pressure. *Invest Ophthalmol Vis Sci*. 2000;41(2):431–442.
48. Tehrani S, Davis L, Cepurna WO, et al. Astrocyte structural and molecular response to elevated intraocular pressure occurs rapidly and precedes axonal tubulin rearrangement within the optic nerve head in a rat model. *PLoS One*. 2016;11(11):e0167364.
49. Burgoyne CF, Quigley HA, Thompson HW, et al. Early changes in optic disc compliance and surface position in experimental glaucoma. *Ophthalmology*. 1995;102(12):1800–1809.
50. Ivers KM, Yang H, Gardiner SK, et al. In vivo detection of laminar and peripapillary scleral hypercompliance in early monkey experimental glaucoma. *Invest Ophthalmol Vis Sci*. 2016;57(9):388–403.
51. Nguyen C, Cone FE, Nguyen TD, et al. Studies of scleral biomechanical behavior related to susceptibility for retinal ganglion cell loss in experimental mouse glaucoma. *Invest Ophthalmol Vis Sci* 2013;54(3):1767–1780.
52. Girard MJA, Francis SJ, Bottlang M, et al. Biomechanical changes in the sclera of monkey eyes exposed to chronic IOP elevations. *Invest Ophthalmol Vis Sci* 2011;52(8):5656–5669.
53. Nguyen C, Midgett D, Kimball E, et al. Age-related changes in quantitative strain of mouse astrocytic lamina cribrosa and peripapillary sclera using confocal microscopy in an explant model. *Invest Ophthalmol Vis Sci*. 2018;59(12):5157–5166.
54. Ma Y, Pavlatos E, Clayson K, et al. Mechanical deformation of human optic nerve head and peripapillary tissue in response to acute IOP elevation. *Invest Ophthalmol Vis Sci*. 2019;60(4):913–920.
55. Beotra MR, Wang X, Tun TA, et al. In vivo three-dimensional lamina cribrosa strains in healthy, ocular hypertensive, and glaucoma eyes following acute intraocular pressure elevation. *Invest Opthalmol Vis Sci*. 2018;59(1):260–272.
56. Pease ME, Oglesby EN, Cone-Kimball E, et al. Scleral permeability varies by mouse strain and is decreased by chronic experimental glaucoma. *Invest Ophthalmol Vis Sci*. 2014;55(4):2564–2573.
57. Steinhart MR, Cone FE, Nguyen C, et al. Mice with an induced mutation in collagen 8A2 develop larger eyes and are resistant to retinal ganglion cell damage in an experimental glaucoma model. *Mol Vis*. 2012;18:1093–1106.
58. Boazak EM, D'Humières J, Read AT, Ethier CR. Compressive mechanical properties of rat and pig optic nerve head. *J Biomech*. 2019;93:204–208.
59. Safa B, Read AT, Ethier CR. Assessment of the viscoelastic mechanical properties of the porcine optic nerve head using micromechanical testing and finite element modeling. *Acta Biomater*. 2021;134:379–387.
60. Downs JC, Suh JKF, Thomas KA, et al. Viscoelastic material properties of the peripapillary sclera in normal and early-glaucoma monkey eyes. *Invest Ophthalmol Vis Sci*. 2023;46:540–546.
61. Quigley HA, Anderson DR. The histologic basis of optic disk pallor in experimental optic atrophy. *Am J Ophthalmol*. 1977;83(5):709–717.
62. Quigley HA, Addicks EM. Chronic experimental glaucoma in primates. II. Effect of extended intraocular pressure elevation on optic nerve head and axonal transport. *Invest Ophthalmol Vis Sci*. 1980;19(2):137–152.
63. Quigley HA, Addicks EM, Green WR. Optic nerve damage in human glaucoma. III. Quantitative correlation of nerve fiber loss and visual field defect in glaucoma, ischemic neuropathy, papilledema, and toxic neuropathy. *Arch Ophthalmol*. 1982;100(1):135–146.
64. Reynaud J, Lockwood H, Gardiner SK, Williams G, Yang H, Burgoyne CF. Lamina cribrosa microarchitecture in monkey early experimental glaucoma: global change. *Invest Ophthalmol Vis Sci*. 2016;57(7):3451–3469.
65. Keuthan CJ, Quillen S, Johnson TV, et al. Regional gene expression in the retina, optic nerve head, and optic nerve of mice with optic nerve crush and experimental glaucoma. *Int J Mol Sci*. 2023;24(18):13719.


Investigative Ophthalmology & Visual Science

66. Pijanka JK, Kimball EC, Pease ME, et al. Changes in scleral collagen organization in murine chronic experimental glaucoma. *Invest Ophthalmol Vis Sci*. 2014;55(10):6554–6564.
67. Cone-Kimball E, Nguyen C, Oglesby EN, Pease ME, Steinhart MR, Quigley HA. Scleral structural alterations associated with chronic experimental intraocular pressure elevation in mice. *Mol Vis*. 2013;19(9):2023–2039.
68. Oglesby EN, Tezel G, Cone-Kimball E, et al. Scleral fibroblast response to experimental glaucoma in mice. *Mol Vis*. 2016:22(1):82–99.
69. Czerpak CA, Quigley HQ, Nguyen TD. Long-term remodeling response in the lamina cribrosa years after IOP lowering by suturelysis after trabeculectomy. *medRxiv* 2023.05.30.23290730, https://www.medrxiv.org/content/10.1101/2023.05.30.23290730v1. Accessed June 4, 2023.